Barrera Vilar, D.; Gasulla Mestre, I.; Sales Maicas, S. (2015). Multipoint two-dimensional curvature optical fiber sensor based on a non-twisted homogeneous four-core fiber. Journal of Lightwave Technology. 33(12):2445-2450. doi:10.1109/JLT.2014.2366556.

Multipoint two-dimensional curvature optical fiber sensor based on a non-twisted homogeneous four-core fiber

D. Barrera, I. Gasulla, and S. Sales

***Abstract*— We have implemented a multipoint two-dimensional curvature optical fiber sensors based on a non-twisted homogeneous four-core fiber. A theoretical approach to the mechanical behavior of these fibers under curvature conditions has been developed. Two shape sensors composed of an array of FBGs inscribed in the four-core have been implemented to corroborate the theoretical analysis with experimental results. The proposed shape sensors is characterized showing the ability to measure the curvature radius, the curvature direction and any external force of uniform and non-uniform curvatures with high accuracy.**

***Index Terms*—Fiber Optic Sensor, Curvature sensor, Fiber Bragg Grating, Multicore**

I. Introduction

MULTICORE optical fibers (MCF) have been intensively studied in the last years within different research areas: high-capacity optical communications [1]; Microwave photonics [2]; and optical sensing, where the spatial diversity inherent to the MCF can be exploited to implement multidimensional sensors in a single fiber device. The measurement of the strain induced to the different cores of the MCF is especially useful to determine both the magnitude and direction of the optical fiber curvature [3-6].

Different approaches have been previously considered to implement curvature and shape sensors using MCFs. References [6-11] proposed the use of a special designed helically twisted MCF composed of an inner core in the center and three outer cores rotating around the central one. This special configuration has brought excellent results to be employed as a shape sensor. The most recent implementations are mostly based on a quasi-continuous single-wavelength low-reflectivity inscribed Fiber Bragg Grating (FBG) that is interrogated using the Optical Frequency Domain Reflectometry (OFDR) technique, obtaining a very high spatial resolution. Non-twisted four-core MCFs have been also proposed to implement curvature sensors [12-13]. Using this type of fiber and with the aim of achieving the best curvature resolution an interferometric interrogation scheme has been proposed in combination of Fabry-Pérot cavities and FBGs [14, 15].

We have studied the curvature sensing properties of MCFs and propose a different approach to the theoretical analysis of these devices. This theoretical analysis may help researchers to analyze the behavior of any non-twisted MCF under curvature conditions independently of the arrangement of the cores in the optical fiber. The theoretical study is completed with the implementation of a shape sensor and the experimental characterization for the measurement of uniform and non-uniform curvatures. The implementation of the shape sensor is made using highly reflective FBGs, placed at different wavelengths and inscribed along a commercial non-twisted homogeneous four-core fiber. The use of highly reflective FBGs prevents the use of techniques like OFDR limiting the maximum numbers of sensing elements but brings also several advantages: a quite remarkable signal to noise ratio (SNR); the use of high-speed commercial FBG interrogators, with measurement rates up to several kHz; and a lower computational cost to determine the shape of the fiber. These advantages imply a significant reduction of the monitoring costs with a reasonable compromise in spatial resolution and curvature resolution.

II. Theoretical analysis

Fig. 1 shows the schematic view of a homogeneous MCF when it is curved. The figure represents a MCF composed of four singlemode cores but the theoretical analysis can be extended to different arrangements of the cores just using the corresponding geometrical relationships between the positions of the cores and the center of the fiber. Since the strain induced to each core depends on the distance between the neutral deformation axis and each core center, the cores closer to the curvature center suffer a compression while the farther ones suffer an elongation. We assume either that the arrangement of the cores is not rotated along the optical fiber or this rotation is slow enough to be considered negligible in short distances. In this case, the strain in the different cores can be used to determine the curvature radius, the curvature

Manuscript received September 7, 2014. This work was carried out with the financial support of the Infrastructure FEDER UPVOV08-3E-008, FEDER UPVOV10-3E-492, the Spanish MCINN through the project TEC2011-29120-C05-05, the Valencian Government through the Ayuda Complementaria ACOMP/2013/146 and the Research Excellency Award Program GVA PROMETEO 2013/012.

D. Barrera, I. Gasulla and S. Sales are with the Optical & Quantum Communications Group, ITEAM research institute, Universitat Politècnica de València. Camino de Vera s/n, 46022 Valencia, Spain (phone: +34 963 877 007; fax: +34 963 879 583; e-mail: dabarvi@iteam.upv.es).

direction and the external strain or temperature.

To analyze the behavior of the curved MCF we can define two planes that are perpendicular to the optical axis and thus define a section of the fiber. If we assume that the curvature produced by the fiber bent is constant within this section, as seen in Fig. 1, these two planes intersect with an angle α. In a first approach we consider that there is no external force applied to the fiber in a way that the strain induced to each one of the cores is given by

$$\varepsilon_i^0 = \frac{\Delta l}{l_0} = \frac{l_i - l_0}{l_0} = \frac{r_i\alpha - r\alpha}{r\alpha} \tag{1}$$

where r is the distance between the curvature center and the center of the optical fiber and r_i, is the distance between the curvature center and each core center with the index i indicating each of the cores in the MCF. The length of the fiber section when it is not bent is given by l_0 that corresponds to the length of the neutral axis in the center of the optical fiber, while l_i is the length of each core after bending the fiber.

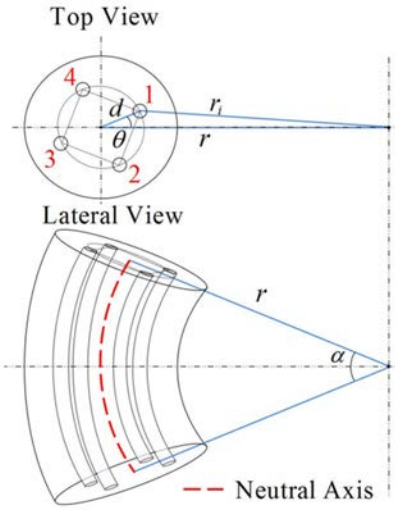

Fig. 1. Schematic top and lateral views of a four-core MCF when it is bent. r is the distance between the center of the optical fiber and the curvature center, θ is the curvature direction and α is the angle between the planes that define the section of the optical fiber.

In a second approach, if we consider an external force F applied to the optical fiber, while being forced to maintain the same curvature, an additional strain ε_F appears that can be defined as

$$\varepsilon_F = \frac{\sigma}{E} = \frac{F}{AE} \tag{2}$$

$$\varepsilon_F = \frac{r\alpha' - r\alpha}{r\alpha} \tag{3}$$

$$\alpha' = \alpha(\varepsilon_F + 1) \tag{4}$$

with σ being the normal stress, E the young's modulus, A the area of the fiber cross section and α' the angle defined by the intersection of the two planes when the external force is applied. Combining the two effects, external force and curvature, the total strain can be calculated as

$$\varepsilon_i = \frac{r_i\alpha' - r\alpha}{r\alpha} = \frac{r_i}{r}(\varepsilon_F + 1) - 1 \tag{5}$$

The previous equations are valid whichever the number or the arrangement of the cores in the MCF. Using the appropriate geometrical relationships between the radius r and the radii r_i, the expressions of the strain in each core can be deduced for the most common MCFs.

Particularizing the equations for a four-core MCF with the cores arranged in the corners of a square at the same distance to the fiber center the expressions for the curvature direction θ, radius r, the external strain and the external strain can be obtained given the different core strains ε_i:

$$\theta = \arctan\left(\frac{(\varepsilon_4 + 1)^2 - (\varepsilon_2 + 1)^2}{(\varepsilon_3 + 1)^2 - (\varepsilon_1 + 1)^2}\right) \tag{6}$$

$$B = \frac{(\varepsilon_1 + 1)^2 + (\varepsilon_3 + 1)^2}{(\varepsilon_3 + 1)^2 - (\varepsilon_1 + 1)^2} \tag{7}$$

$$r = d\left(B\cos\theta + \sqrt{B^2\cos^2\theta - 1}\right) \tag{8}$$

$$\varepsilon_F = \sqrt{\frac{(\varepsilon_3 + 1)^2 - (\varepsilon_1 + 1)^2}{4\frac{d}{r}\cos\theta}} - 1 \tag{9}$$

where d is the distance between the center of the cores and the center of the optical fibre and the parameter B is introduced to simplify the formulation. Note that Eq. (6), (7), (8) and (9) follow the numeration of the cores as shown in Fig. 1.

III. Implementation

The shape sensor has been implemented using a wavelength multiplexed array of highly reflective FBGs inscribed along a commercial homogeneous MCF. The use of wavelength multiplexed highly reflective FBGs limits the maximum number of sensing elements but contributes to a reduction of the interrogation setup cost, a significant increase of the interrogation speed and a higher SNR with a reasonable compromise in spatial resolution and curvature resolution that may be interesting for short devices. The MCF we have used to implement the shape sensor has been provided by Fibercore and is composed of four identical singlemode cores arranged in the corners of a 36-µm-side square lattice. In this application it is desirable for all the inscribed FBG sensors to be similar in terms of spectral characteristics: reflectivity, Full-Width at Half Maximum (FWHM) and apodization. This simplifies the Bragg wavelength detection in the different cores. However, the simultaneous inscription of FBGs in all the cores is a challenging process as it is hampered by several limitations such as the inhomogeneity of the laser fluence along the multiple cores and the lens effect of the optical fiber [8].

The MCF used for the shape sensor implementation is designed for high-capacity communications and its photosensitivity is very low. For inscribing the FBGs the optical fiber has been previously hydrogen-loaded at 20-bar pressure for two weeks at room temperature to increase its photosensitivity and the beam from an Argon-ion frequency-doubled laser has been defocused to irradiate all the cores at the same time. The inscription technique is based on the use of a uniform phase mask combined with a precise relative movement between the phase mask and the optical fiber [16]. The irradiation is divided into two sub-irradiations performed at precise positions along the FBG. The irradiation times of the two sub-irradiations are the same and constant along the whole length of the FBG. The positions where the optical fiber is irradiated are determined by a composition of two different displacements: the first one, related to the period of the phase mask, increases the length of the FBG; the second one is designed to introduce a phase shift between the two sub-irradiations controlling the apodization of the FBG. This process irradiates each position along the FBG multiple times what under controlled conditions of irradiation time and spacing leads to a state of saturation in the refractive index change in all the cores. The saturation of the refractive index does not directly imply the saturation of the FBG reflectivity since it also depends on the length of the FBG and the apodization used [17]. The apodization of the FBG spectra can be important when using shorter FBGs, with a broader FWHM, and when the number of FBGs in the shape sensor limits the spectral spacing between FBGs because the sidelobes can interfere with the neighbor FBG spectrum and lead to an erroneous Bragg wavelength determination.

The number of FBGs in the shape sensor depends on the length of the device, the length of the FBGs and the nature of the curvatures to be measured. For slow-varying or nearly constant curvatures, the spacing of FBGs can be increased. In contrast, for non-uniform curvatures, the strain along the fiber can experience rapid changes. In this case, the number of sensing points should be increased and the distance between FBGs should be reduced in order to retrieve the strain evolution along the optical fiber. At the same time, the length of the FBGs should be reduced to minimize the non-uniformity of the strain along the FBGs and prevent a chirp effect that can modify their spectral properties.

Taking into account the previous considerations, two different sets of shape sensors have been implemented. The first sensor set is composed of an array of four FBGs. Both the length of the FBGs and the distance between them has been set to 1 cm, giving a total sensor length of 7 cm. These sensor sets have been used for characterization of the overall shape sensor and the measurement of constant curvatures. The second set of sensors is composed of an array of 15 FBGs. Both, the length of the FBGs and the space between them have been set to 2 mm, resulting in a 58-mm long sensor. The shorter length of the FBGs and spacing between them, characteristic of this second sensor configuration, have allowed to measure non-uniform curvatures. All the inscribed FBGs have a Gaussian apodization in order to reduce the reflectivity of the side lobes of the optical spectrum.

Finally, the sensors have been connectorized to four standard singlemode single-core optical fibers in order to interrogate all the cores at the same time using a four-channel MCF fan-out device from Optoscribe and a commercial FBG interrogator from Micron Optics.

IV. Results

A set of different polymer molds and their respective counter molds with constant curvature have been designed and fabricated in order to characterize the implemented sensors. The curvature of these polymer molds varies from 2.9 m^{-1} to 26.17 m^{-1}. In a first approach, we have characterized constant curvatures using the sensors composed of arrays of four FBGs. After the characterization, we use a combination of two of these polymer molds to measure changes in the curvature. In this case, we resorted to the sensors composed of arrays of 15 FBGs to monitor these non-uniform curvatures.

A. Uniform curvatures

The setup used to characterize the shape sensor is depicted in Fig. 2a. The optical fiber is vertically suspended with a small weight attached at the bottom end. This weight maintains the optical fiber straight and subjected to a nearly constant strain. The polymer molds are fastened to a first rotation stage placed on the top of a post. The measurement procedure first fixes the direction of curvature using a second rotation stage placed at the base of the characterization system. Then, the optical fiber is clamped to the upper side of the polymer mold. This rotation stage is then actuated in order to apply the desired curvature. The polymer molds are long enough to place the four FBGs. The sensor is characterized using molds with different curvatures while rotating the curvature direction θ in steps of 10º. Figure 2b displays both the magnitude r and direction θ of the curvature obtained by the first FBG when a polymer mold with a curvature of 5.81 m^{-1} (radius r = 172 mm) is used. The experimental results show a good agreement with the curvature of the mold. The standard error is less than 1.6% in the range of curvatures measured. The other three FBGs show nearly identical results and thus have not been displayed for the sake of clarity. The radius resolution of the sensor and the interrogation setup has been evaluated during the characterization of uniform curvatures, obtaining a non-averaged value of 0.1 mm under nearly constant temperature conditions.

Regarding the determination of the direction of curvature θ we have obtained an accuracy of 96.7% in the FBG located closer to the clamp, where small fluctuations were mainly produced by the slight rotation that can be experienced by the optical fiber when it is clamped to the mold surface.

In general, a Coordinate Reference System (CRS) is needed for many applications in order to unambiguously determine the curvature direction. Specially designed optical fibers like the helically twisted fiber use the shear stress produced when the fiber is twisted to discriminate the curvature and torsion of the optical fiber. The shear stress depends on the distance to the center of the optical fiber, for this reason with the four-core optical fiber used with all the cores at the same distance to the fiber center the shear stress produces the same

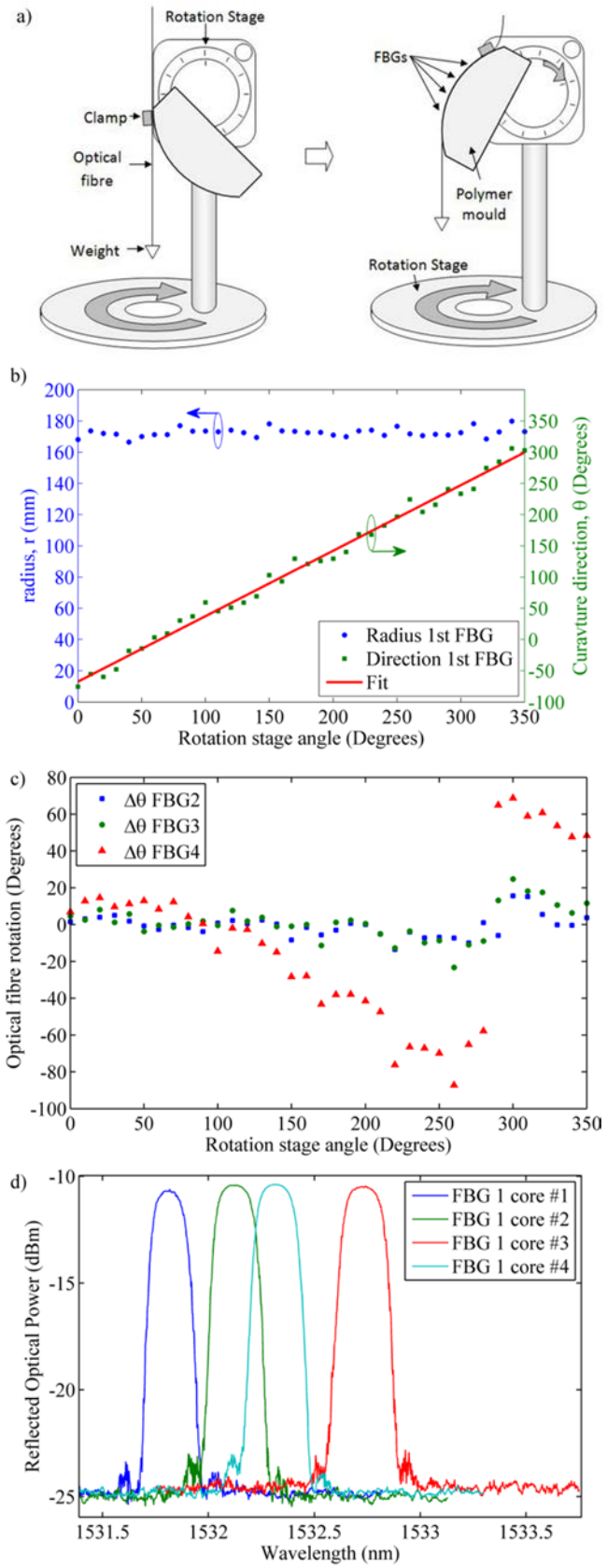

Fig. 2. a) Characterization setup for the measurement of uniform curvatures. b) Measured radius r and direction θ for uniform curvatures. c) Curvature direction differences between the first and the other FBGs. d) Optical spectra of one of the four FBGs along each of the cores.

strain in all the cores preventing the twist and curvature to be discriminated. In order to define the CRS the rotation of the optical fiber is usually prevented.

During these experimental tests the fiber torsion is not prevented in order to not include any external element and preserve the sensing properties. For this reason, in Fig. 2b the small changes in the curvature direction are mainly produced by the rotation of the optical fiber. With this fiber the curvature and twist cannot be distinguished without certain knowledge about the curvature to be measured. It is worth mentioning that when the optical fiber is maintained in a plane and no changes in the concavity along the entire length of the fiber are observed, even if the curvature radius is not constant, the direction of curvature is known and in consequence, any change observed in the direction of curvature corresponds to the torsion of the optical fiber. The same occurs in the characterization setup shown in fig. 2a where the curvature direction is known. Fig. 2c shows the difference in the measured curvature direction between the curvature direction of the first FBG, close to the clamp and shown in Fig. 2b, and the one measured by the other three FBGs. As it was expected, since the rigidity of the optical fiber is low, the fiber torsion strongly depends on the distance to the force that produces the torsion. In our case, the fourth FBG is the one that is more distant to the clamp and closer to the weight showing higher curvature direction differences. For two consecutive FBGs the maximum unambiguous rotation is 2π but it is possible to increase this measurable rotation range increasing the number of FBGs.

The optical spectra of one of the FBGs along the four cores of the MCF are shown in fig. 2d. The obtained maximum reflectivity for all the FBGs varies from the 87% to the 95% of the injected light (-10 dBm) and their FWHM from 0.17 nm to 0.24 nm.

The strain ε_F produced by the 4.1 g weight placed at the end of the optical fiber has been measured in each one of the four FBGs throughout the whole characterization process, obtaining values placed between 35 με and 42 με that match very well the predicted theoretical value calculated from Eq. (2).

B. Non-uniform curvatures

In order to achieve a higher spatial resolution we have resorted to the second set of sensors implemented with arrays of 15 FBGs to measure the transition between two different curvatures with opposite concavity, as shown in Fig. 3a. Since this setup forces the optical fiber to be bent in two opposite directions, we are able to measure the changes in the curvature magnitude experienced from one constant curvature to a different constant curvature. The counter-molds have been used to gently force the fiber to follow the desired transition but, in this case, we have not applied other additional forces F to the sensor. The measurements have been taken using different combinations of curvatures while changing the position of the shape sensor related to the transition between the molds.

Fig. 3b shows the optical spectra of one of the FBGs along the four cores of the optical fiber. It can be observed the great similitude in the FBG spectra along the different cores. The spectra of all the FBGs have been measured using a sweep

laser source with a -10 dBm output power and an Optical spectrum analyzer. The reflectivity of all the 2 mm long FBGs vary from 18% to 23% of the injected light achieving a SNR in reflection higher than 20dB in all the cases facilitating the detection of the FBGs and the Bragg wavelength determination. Despite other apodizations can also be used, the use in this case of the Gaussian apodization contributes to reduce the sidelobes level near the noise level.

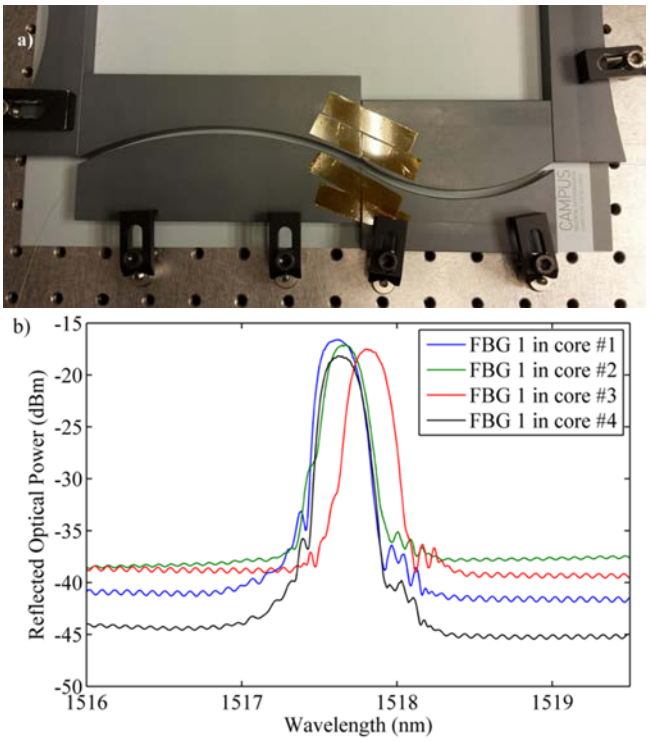

Fig. 3. a) Characterization setup for the measurement of non-uniform curvatures. b) Optical spectra of one of the FBGs along each core in the MCF.

Fig. 4 represent the results obtained for the transition between a first constant curvature of 11.3 m^{-1} (radius of 88.4 mm) and a second constant curvature of 5.81 m^{-1} (radius of 172 mm). A shape-preserving piecewise cubic Hermite interpolation has been added to facilitate the visualization of the experimental data. We observe in Fig. 4a that the transition between both molds is located between the 6^{th} and 7^{th} FBGs, which in fact shows a much higher curvature radius *r*. For the sake of clarity, the two constant radius values have been represented in the same figure. It is worth to note that in the proximities of the transition the magnitude of the curvature does not match the values of the constant curvature radii. This particular behavior is a consequence of some freedom experienced by the optical fiber in the transition section since the force applied by the counter-molds cannot be too high in order to prevent any damage to the fiber. The maximum measured radius, which theoretically corresponds to infinite, is in practice limited by the physical dimensions of the FBG and the precision reached in the measurement procedure. Since the optical fiber is not affected by any external force, the measured values of the strain ε_F are kept below 10 με along the whole length of the shape sensor and this small strain is consequence of the friction between the optical fiber and the polymer mold.

The curvature direction behavior displayed in Fig. 4b shows the expected 180º direction transition. In this case we know the curvature direction is parallel to the plane of the FBG. Under these circumstances there twist of the fiber and curvature direction can be distinguished. While curvature direction changes produce in this case direction changes of 180 degrees the twist of the fiber corresponds to the smaller fluctuations in the curvature direction allowing to perfectly reconstruct the shape of the non-uniform curvature.

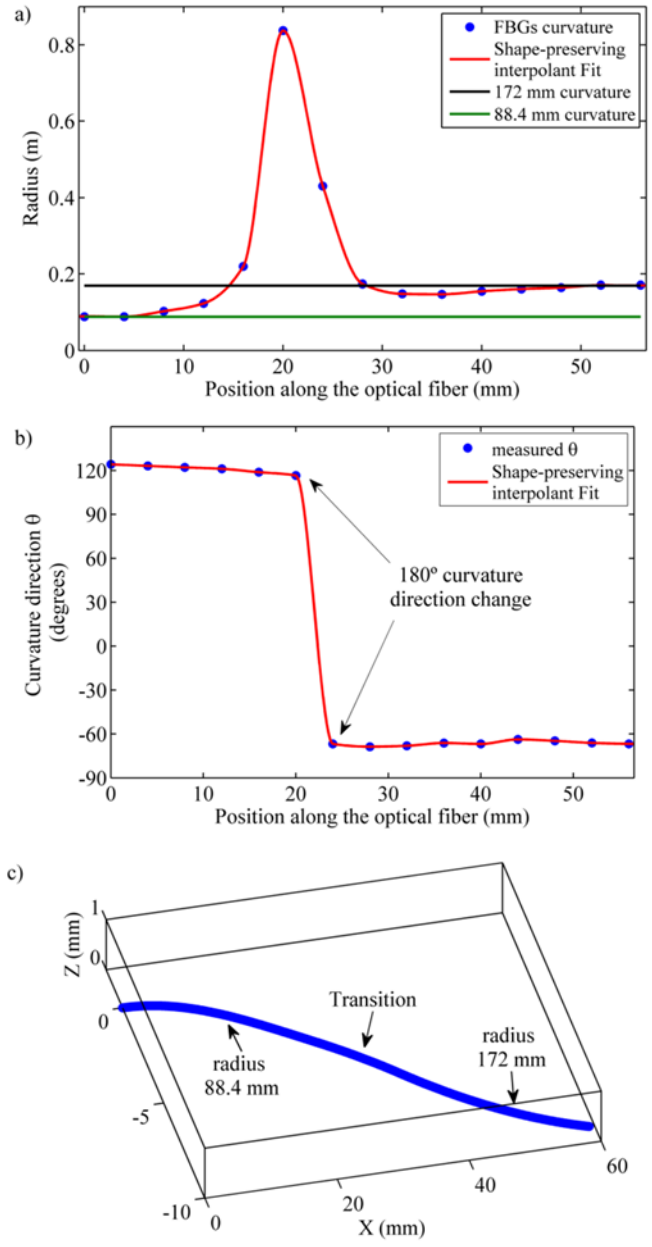

Fig. 4. a) Measured radius *r* along the sensor. b) Measured curvature direction θ along the sensor. c) Reconstruction of the sensor shape.

The reconstruction of the shape of the optical fiber shown in Fig. 4c is made from the measured curvature magnitude and

direction and using a combination of common image rotation and displacement matrices.

V. CONCLUSION

We have implemented a multipoint two-dimensional curvature optical fibre sensors based on a non-twisted homogeneous four-core fiber. A theoretical approach to the mechanical behavior of these fibers has been developed under curvature conditions. The theoretical study is particularized for the four-core MCF used and has been corroborated with the implementation and later characterization of a shape sensor for the measurement of uniform and non-uniform curvatures. The implementation of the shape sensor is made using apodized highly reflective FBGs, placed at different wavelengths and inscribed along a commercial non-twisted homogeneous four-core fiber. The size and spacing of the FBGs in the array have been considered and two sets of sensors have been implemented: a first one implemented with arrays of 4 FBGs that features a lower spatial resolution and is aimed at measuring nearly constant curvatures; and a second one composed of arrays of 15 FBGs featuring a higher spatial resolution that results more appropriate for non-uniform curvatures. The characterization of the shape sensor using constant curvatures has shown a good performance obtaining a standard error under 1.6% in the range of curvatures measured. We have also measured non uniform curvatures using the transition between two different uniform curvatures. The results showed an excellent agreement with the expected values. The knowledge about the nature of the curvature to be measured allows us to distinguish between curvature direction and twist of the optical fiber allowing the successful reconstruction of the shape of the optical fiber.

REFERENCES

[1] D. J. Richardson, J. M. Fini, and L. E. Nelson, “Space division multiplexing in optical fibers,” *Nat. Photonics*, vol. 7, no. 5, pp. 354-362, Apr. 2013.

[2] I. Gasulla and J. Capmany, “Microwave Photonics Applications of Multicore Fibers,” Photonics J. vol. 4, no. 3, pp. 877-888, Jun. 2012.

[3] D. Barrera, and S. Sales “Multipoint two-dimensional curvature optical fibre sensor” *Proc. SPIE*, vol. 9157, 91570A, Jun. 2014;

[4] K. Omichi, H. Uemura, K. Sasaki, K. Takenaga, R. Goto, S. Matsuo, K. Saitoh, and R. Yamauchi, “Multi-core to 7 single-core-fibers fan-out device with multi-core fiber pigtail connector” *Proc. SPIE*, vol. 9157, 915732, Jun. 2014.

[5] M. Napierala, M. Murawski, M. Szymanski, L. Ostrowski, L. Szostkiewicz, P. Mergo, L. Jaroszewicz, and T. Nasilowski; “Optical fiber elements for addressing individual cores in multicore optical fiber sensors” *Proc. SPIE*, vol. 9157, 915739, Jun. 2014.

[6] Luna Innovations Inc., “Fiber optic shape sensing. Current state of technology,” Luna Innovations Inc., Jun. 2013. Available: http://lunainc.com/wp-content/uploads/2012/08/SS-00021-D-TS_FiberOptic-Shape-Sensing-Snapshot+TechBackground_Rev003.pdf

[7] C. Askins, G. Miller, and E. Friebele, “Bend and Twist Sensing in a Multiple-Core Optical Fiber,” in *Proc. OFC/NFOEC*, San Diego, CA, 2008, paper OMT3.

[8] C. Askins, T. Taunay, and G. Miller, “Inscription of fiber Bragg gratings in multicore fiber,” in *Proc. BGPP*, Quebec City, 2007, paper JWA39.

[9] P. S. Westbrook, K. S. Feder, T. Kremp, T. F. Taunay, E. Monberg, J. Kelliher, R. Ortiz, K. Bradley, K. S. Abedin, D. Au, and G. Puc, “Integrated optical fiber shape sensor modules based on twisted multicore fiber grating arrays,” *Proc. SPIE*, vol. 8938, 89380H. Feb. 2014.

[10] R. Duncan, “Sensing Shape: Fiber-Bragg-grating sensor arrays monitor shape at a high resolution” *SPIE Newsroom*, Sept. 2005. Available: http://spie.org/x15732.xml

[11] http://www.4fos.com/

[12] A. Fender, W. N. MacPherson, R. Maier, J. S. Barton, D. S. George, R. I. Howden, G.W. Smith, B. Jones, S. McCulloch, X. Chen; R. Suo, L. Zhang and I. Bennion, “Two-Axis Temperature-Insensitive Accelerometer Based on Multicore Fiber Bragg Gratings,” *IEEE Sens. J.* vol. 8, no. 7. pp. 1292-1298, Jul. 2008.

[13] G. Flockhart, W. MacPherson, J. Barton, J. Jones, L. Zhang and I. Bennion, “Two-axis bend measurement with Bragg gratings in multicore optical fiber,” *Opt. Lett.* vol. 28, no. 6, pp. 387-389, Mar. 2003.

[14] G. A. Cranch, G. M. H. Flockhart, W. N. MacPherson, J. S. Barton, and C. K. Kirkendall, “Ultra-high-sensitivity two-dimensional bend sensor,” *Electron. Lett.*, vol. 42, no. 9, pp. 520-522, Apr. 2006.

[15] G.M.H. Flockhart, G.A. Cranch and C.K. Kirkendall, “Differential phase tracking applied to Bragg gratings in multi-core fibre for high accuracy curvature measurement,” *Electron. Lett.* vol. 42, no. 7, pp. 390-391, Mar. 2006.

[16] M. J. Cole, W. H. Loh, R. I. Laming, M. N. Zervas, and S. Barcelos, "Moving fibre/phase mask-scanning beam technique for enhanced flexibility in producing fibre gratings with uniform phase mask," *Electron. Lett.*, vol. 31, no.17, pp. 1488-1490, Aug. 1995.

[17] A. Othonos, and K. Kalli, *Fiber Bragg Gratings: Fundamentals and Applications in Telecommunications and Sensing*, Artech House Optoelectronics Library, Boston, MA, USA, 1999.